CHAPTER V
REVIEWS ON (HYPER) (LIGHT) NUCLEI

The previous chapter has already pointed out that cluster formations are important for critical phenomena of the medium and the EoS studies. Also, the tension between formation mechanisms arises due to the different space-time pictures in the heavy-ion collisions. In this chapter, we will review on the cluster formations ranging from the normal nuclei to the hypernuclei by discussing their roles in various studies and the available formation mechanisms on the markets.

5.1 Role of (Hyper)Nuclei Formation

Nuclei or clusters, such as deuteron, triton, and Helium-3, are the bound state of two or more nucleons. The studies of these particles are crucial for a broad range of physics from the nuclear physics (Knoll et al., 1982; Sun et al., 2017; Zhu et al., 2015; Oh and Ko, 2007) to the astrophysics (Hagedorn, 1960; Butler and Pearson, 1961; Carlson et al., 2014; Hou et al., 2017; Most et al., 2023).

In the context of the heavy-ion collisions, they are important probes for the critical behavior and the EoS due to their sensitivity to the medium (Andronic et al., 2011; Blaschke et al., 2020; Knoll et al., 1982; Hagel et al., 2012; Yang et al., 1984). This is attributed to the nature of the bound state and the final stage observables. They can be reflective to the various medium effects from the early to final stage of the collisions. For example, beam energy and initial geometries can lead to the different temperatures and densities affecting the cluster formations at the final stage (Csernai and Kapusta, 1986; Hagel et al., 2012). The correlations and fluctuations of the baryon at the critical point also lead to change in their multiplicities (Knoll et al., 1982; Bertsch and Cugnon, 1981; Oliinychenko, 2021).

In the context of astrophysics and cosmology, these clusters, particularly the light nuclei, play a critical role in understanding the early universe (Yang et al., 1984) providing a strong support on the most famous cosmological models, i.e., Big Bang models (Alpher and Herman, 1948; Yang et al., 1984; Malaney and Mathews, 1993; Pospelov and Pradler, 2010). Also it has been postulated that the antideuterons in space could

be used to trace and investigate the candidate and nature of dark matter (Korsmeier et al., 2018; Bellini, 2022; Fuke et al., 2005; Ibarra and Wild, 2013; Aguilar et al., 2016). .

However, the research on these clusters has been recently highlighted again due to the fact that their fundamental structures and formations could serve as a basis for studying hypernuclei (Cho et al., 2017; Andronic et al., 2018; Braun-Munzinger and Dönigus, 2019). The hypernuclei are the bound state between nucleons with a least one strange baryon called hyperon. These hypernuclei could extend our understanding of the QCD matter in both nuclear physics and astrophysics aspects as well.

Furthermore, since the strangeness is only produced from the early stage of the collisions, these hypernuclei also carry information at the very initial stage of the collisions. They are also subjected to the correlations and fluctuations of the medium due to their bound state nature. Particularly, the goal for investigating the hypernuclei in the nuclear medium is to understand their internal structures and interactions. However, at high collision energies, these hypernuclei are very rare making their experimental data situations very limited.

This motivates most of the heavy-ion collision facilities to design lower energies collision to enhance the strangeness productions in the nuclear medium (Schaffner-Bielich and Gal, 2000; Andronic et al., 2011). These created environments correspond to the neutron stars and binary neutron star mergers. The presence of hyperons in these compact stellar objects can influence the neutron star EoS (Balberg et al., 1999; Chatterjee and Vidaña, 2016; Oertel et al., 2016) through hyperon-nucleon interactions (Nagels et al., 1977; Nagels et al., 1979; Shinmura et al., 1984; Fujiwara et al., 1996a; Fujiwara et al., 1996b; Nemura et al., 2000; Hildenbrand and Hammer, 2019) and ultimately affecting the maximum mass and radius of these stellar objects (Bombaci, 2017; Özel and Freire, 2016; Lattimer, 2021). This suggests that the hypernuclei could also serve as sensitive probes for the EoS especially around neutron star density.

The investigation on their internal interactions are also important to their formation mechanisms. One could argue that these normal nuclei and hypernuclei are formed from the same mechanism. The investigation on the formation mechanism from the normal nuclei could also be crucial to understand the nature of the hyperon interactions.

The following sections will delve deeper into these highlighted topics, exploring the detailed mechanisms and implications of (hyper)nuclei studies in various physical contexts (for more detailed reviews Ref. (Dönigus, 2020)).

Big Bang Nucleosynthesis

Big Bang Nucleosynthesis (BBN) is one of the eras of the early universe where a larger amount of light atomic nuclei are continuously created. It was postulated to happen a few minutes after the Big Bang (Alpher and Herman, 1948; Malaney and Mathews, 1993). Originally, while the universe was cooling down, many light nuclei could be formed but hot universe with energetic nucleons, also destroyed them continuously. Only until the universe is cool enough such that it allows deuterons to survive. This is one of the most important threshold in the BBN, the so-called "deuteron bottleneck". A large amount of light nuclei can be produced with these deuterons as their constituent in which inducing an enormous nuclear chain reaction to form other heavier nuclei (Pospelov and Pradler, 2010).

Interestingly, most of the abundance of deuterium observed in the universe today is accounted from the BBN era. By investigating the primordial deuteron yields from the coalescence model along with the constraints on the density and composition of baryonic matter in the early universe from the cosmic microwave background, we can obtain the most valuable evidence for supporting the BBN model (Alpher and Herman, 1948; Yang et al., 1984; Pospelov and Pradler, 2010).

Furthermore, the same argument can also be applied to the heavy-ion collisions. The cluster formation from the thermal model provides a contradict picture with the deuteron bottle neck argument leading to the so-called "snow ball in hell" where these loosely bound clusters are directly emitted from the hot fireball at the chemical freeze-out with temperature $T_{chem} \geq 100$ MeV. However, in this thesis, we will eventually point out that the coalescence model could provide more consistent pictures between the emission source geometries, BBN, and other arguments like isospin fluctuations.

Potential Signal of the Critical point

When the medium reaches the critical point, it induces a significant change to the thermodynamics properties leading to the divergence of the correlation length, susceptibility, and fluctuations particularly in conserved quantities like baryon number, electric charge, or strangeness. The fluctuation of these conserved observables has been extensively studied both theoretically and experimentally through event-by-event fluctuations and correlations (Sun et al., 2017; Stephanov et al., 1999; Stephanov, 2009; Skokov et al., 2013; Luo and Xu, 2017; Mrówczyński and Słoń, 2020).

Measurements from the Beam Energy Scan (BES) program by the STAR Collaboration have reported clear deviations from unity or shown a non-monotonic behavior in the energy-dependence of event-by-event fluctuations, such as fourth-order fluctuations ($\kappa\sigma^2$) of the net-proton number, which could indicate a critical behavior (Adamczyk et al., 2014). This critical behavior manifests in various final state observables, including $\eta/s \propto d/p$ (Andronic et al., 2009; Braun-Munzinger and Dönigus, 2019; Andronic et al., 2017), and the slope of harmonic flows of light clusters (Hartnack et al., 1994). These observations are sensitive to the correlations and fluctuations near the critical point.

Moreover, due to the fact that the constituent nucleons are subjected to the baryon conservation, the critical fluctuations and the correlation length will be reflected by the relative densities between nuclei and nucleons at kinetic freeze-out in heavy-ion collisions, e.g., $\mathcal{O}(d/p)$, $\mathcal{O}(tp/d)$ and $\mathcal{O}(p^3He/d)$. These ratios are expected to reflect pure contributions from proton-neutron correlations and baryon fluctuations (Oliinychenko, 2021; Liu et al., 2020).

Relation to Dark Matter

The estimated ratio of, e.g., d/p abundances aligns reasonably well with the observable number of baryons in the universe today (Yang et al., 1984; Hou et al., 2017). This implies that there isn't a significant unseen source for baryons. However, the observations also suggest that a large quantity of matter is necessary to explain the gravitational behavior of galaxies and their halos, at least 10 times the mean density of the visible baryons (Aguilar et al., 2016). Thus, this indicates that this missing mass is not made of ordinary matter, but the so-called dark matter.

The AMS experiment aims to measure the flux of antinuclei in space (Fuke et al., 2005; Ibarra and Wild, 2013; Aguilar et al., 2016). It has been postulated that dark matter annihilation could produce the $N\bar{N}$ which then potentially form the antinuclei (Carlson et al., 2014; Korsmeier et al., 2018; Bellini, 2022; Šerkšnyté et al., 2022) where the formation rates of these antinuclei are theoretically estimated by the coalescence model that is also applied in heavy-ion collisions (Nagle et al., 1994; Bleicher et al., 1995; Abelev et al., 2010; Zhu et al., 2015; Chen et al., 2018).

Understanding the correct mechanism for cluster formation from heavy-ion collisions might help us provide the correct estimated production rate of these antinuclei.

5.1.1 Hypernuclei

One of the important aspects for cluster studies in heavy-ion collisions is the role of strange quarks and strange hadrons in the medium. These strange quarks are only produced after the medium reaches the QGP stage and only after the hadronization passes, their bound states are then allowed to form. From this point, one can foresee that the hypernuclei could be influenced by various factors such as strong interactions, decays, fluctuations, and re-scattering throughout the evolution. However, these final stage observables can also be seen as information carrier from the early stages of the QGP (Koch et al., 1986; Soff et al., 1999).

Despite significant theoretical advancements and the fact that available models could already accurately estimate hyperon and hypernuclei behaviors and spectra, several topics remain open for investigation (Rufa et al., 1990; Gibson and Hungerford, 1995).

One of such topics is the hypertriton structure and its dependence on system size (Acharya et al., 2022). Measurements of the hypertriton lifetime, which is close to that of Λ hyperons, suggest a structure consisting of a deuteron core and a loosely bound Λ (Juric et al., 1973; Abelev et al., 2010; Adam et al., 2016; Dönigus, 2020; Andronic et al., 2018). Understanding the correct hypertriton structure requires a consistent wavefunction, and interactions between its constituents, such as ΛN or ΛNN interactions and even $\Lambda\Lambda$N interactions (Nagels et al., 1977; Nagels et al., 1979; Shinmura et al., 1984; Fujiwara et al., 1996a; Fujiwara et al., 1996b; Nemura et al., 2000).

The main challenge in understanding hyperon-nucleon interactions is the lack of experimental data. Thus for the current trend for most facilities will focus on these hypernuclei studies especially toward the lower energy regime (lower temperature but higher density) where hypernuclei yields are expected to be enhanced and the environments are suitable for studying their internal interactions through correlations (Bertsch and Cugnon, 1981; Lisa et al., 2005; Mihaylov et al., 2018; Acharya et al., 2019). Future facilities like FAIR, PANDA, and HADES will conduct research with particular interest in this regime for hypernuclei physics (Pochodzalla, 2005; Ablyazimov et al., 2017; Gal et al., 2016; Almaalol et al., 2022) aiming to investigate their structure, the underlying internal interactions such as hyperon-nucleon and hyperon-hyperon interactions, and the weak decays of these objects.

These hypernuclei structure and internal interaction studies have direct implications to the neutron stars EoS (Huth et al., 2022). Since the attractive and repulsive

nature of these interactions will influence the balance of the Fermi pressure. Inside the neutron stars, it is expected the presence of hyperons and hypernuclei. However, the inclusion from their contributions from various models result in a strong softening of the EoS (Balberg et al., 1999; Chatterjee and Vidaña, 2016; Oertel et al., 2016). The maximum masses in these cases could never reach the observed neutron stars masses of around $2M_{\odot}$ (Biswas, 2021). While the pure neutron star model exhibits a too stiff EoS leading to the always larger possible masses for pure neutron stars. Thus, a comprehensive understanding of the effects of hypernuclei and their constituent hyperons is also crucial for understanding the properties of matter under extreme conditions, not only in heavy-ion collisions but also in contexts such as the early universe (Rafelski and Yang, 2022) and the cores of neutron stars (Özel and Freire, 2016; Lattimer, 2021).

5.2 Cluster Formation Mechanisms

To accurately predict the yield of nuclei formation, understanding the underlying mechanisms responsible for this process is important. In this section, we will introduce the most successful and well-known mechanisms for nuclei formation. Despite their successes, each model has its own interpretations, leading to debates over which mechanism is realized in nature.

5.2.1 Thermal productions

Thermodynamic models have been extensively used to study the macroscopic properties of strongly interacting matter over a broad range of energies. These statistical thermal models are applicable when the system has reached its equilibrium. In the sense of heavy-ion collisions, this equilibrium refers to the stage of chemical freeze-out (Andronic, 2014; Cleymans et al., 2006). In this section, we will introduce the setup of the model for nuclei production by following the explanation presented by Ref.. (Kapusta, 1980; Vovchenko and Stoecker, 2019) and discuss some drawbacks (see also Ref. (Mrowczynski, 2017)).

The basic idea of the thermal model is to treat each particle species as a non-interacting gas. The schematics for the thermal model is shown in Figure 5.1.

Inside the fireball, all kinds of particles (hadrons and clusters) can form. The nuclei are treated, like other particles, as free particles inside a volume V_{chem} characterized by temperature T_{chem} and chemical potential $\mu_{chem,i}$. The distribution of particle i

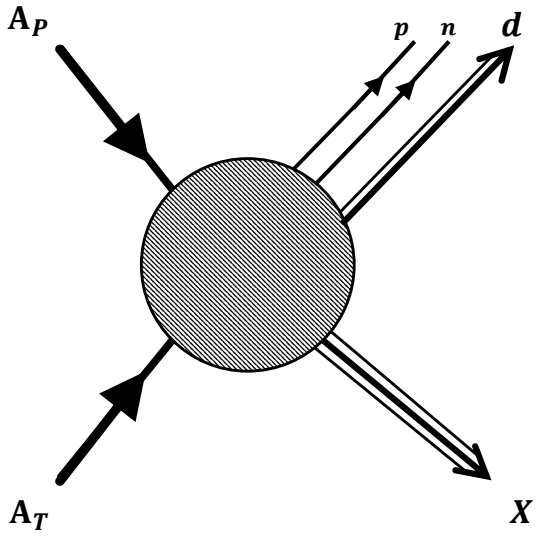

Figure 5.1 The schematic for a particle production from a thermal model. A projectile A_P and a target nucleus A_T exchange energy and momentum upon collision. All particles X, p and n, are emitted directly from the fireball including the composited particle d. This hadronization occurs at chemical freeze-out. The figure is adopted from Ref. (Kapusta, 1980)

can be described as:

$$\frac{d^3N_i}{dp_i} = \frac{(2S_i+1)}{(2\pi)^3}V\left[\exp\left(\frac{(p_i^2+m_i^2)^{1/2}-\mu_i}{T}\right)\pm 1\right]^{-1}, \qquad (5.1)$$

where S_i is the spin multiplicity of the particle, and $\pm$ depends on whether the particle is a fermion or boson.

The particle distribution function can then be rewritten in terms of the Milne momentum coordinates, while the spatial coordinates are integrated and yield the three-volume V. It is also possible to introduce Milne-coordinates for coordinate space $(t, x, y, z) \rightarrow (\eta, r_T, \tau, \theta)$,

$$\frac{d^3N}{dm_T dy d\phi} = \frac{gV}{(2\pi)^3}Em_T\frac{1}{e^{\beta(E-\mu)}\pm 1} \qquad (5.2)$$

$$= \frac{gV}{(2\pi)^3}\frac{m_T^2\cosh(y)}{e^{\beta(m_T\cosh(y)-\mu)}\pm 1} \qquad (5.3)$$

If the bulk evolution is symmetric with respect to ϕ, one can integrate over the azimuthal angle and obtain the particle distribution as a function of y and m_T:

$$\frac{d^2N}{dm_T dy} = \frac{gV}{(2\pi)^2} \frac{m_T^2 \cosh(y)}{e^{\beta(m_T \cosh(y) - \mu)} \pm 1} \tag{5.4}$$

From here on one can calculate the transverse momentum spectrum of a given particle species or the rapidity distribution. Moreover, integration over y and m_T yields the total number of particles.

$$N = \frac{gV}{(2\pi)^2} \int_{-\infty}^{\infty} dy \int_{m}^{\infty} dm_T \frac{m_T^2 \cosh(y)}{e^{\beta(m_T \cosh(y) - \mu)} \pm 1} \tag{5.5}$$

The thermal description can provide a good estimate for normal hadron productions, see figure 5.2. However, the estimated (anti)cluster or hypernuclei yields are usually poor (on the logarithmic scale). Nevertheless, a simple thermal model can still give us a lot of insight on the particle productions from a very wide spectrum ranging from SPS to RHIC energies without any need to introduce more parameters (Andronic et al., 2010).

Various extensions of the ideal gas picture have been discussed mostly within the excluded volume (Rischke et al., 1991; Yen et al., 1997; Yen and Gorenstein, 1999), where the effects of repulsive hadronic interactions at short distances are introduced. Another extension is the quantum van der Waals model (Vovchenko et al., 2015; Vovchenko et al., 2017a; Vovchenko et al., 2017b), which allows to include both the repulsive and attractive interactions between hadrons. Recently, repulsive interactions have received renewed interest in the context of lattice QCD data on fluctuations of conserved charges. In addition, the fugacity free parameters sometimes are introduced and used to describe how the presence of particles deviates from ideal gas behavior due to interactions (Koch et al., 1986; Rafelski, 1991; Letessier and Rafelski, 1999). A modified pressure term accounts for the chemical potential and reflects the departure from equilibrium conditions. Especially for hypernuclei, there is a strong enhancement visible at low energies that can be understood as an interplay of the medium T, μ_i, and canonical effects. This is of particular interest for low energy facilities where collisions occur at chemical potential, like the upcoming FAIR facility (Friman et al., 2011; Ablyazimov et al., 2017; Durante et al., 2019; Bzdak et al., 2020).

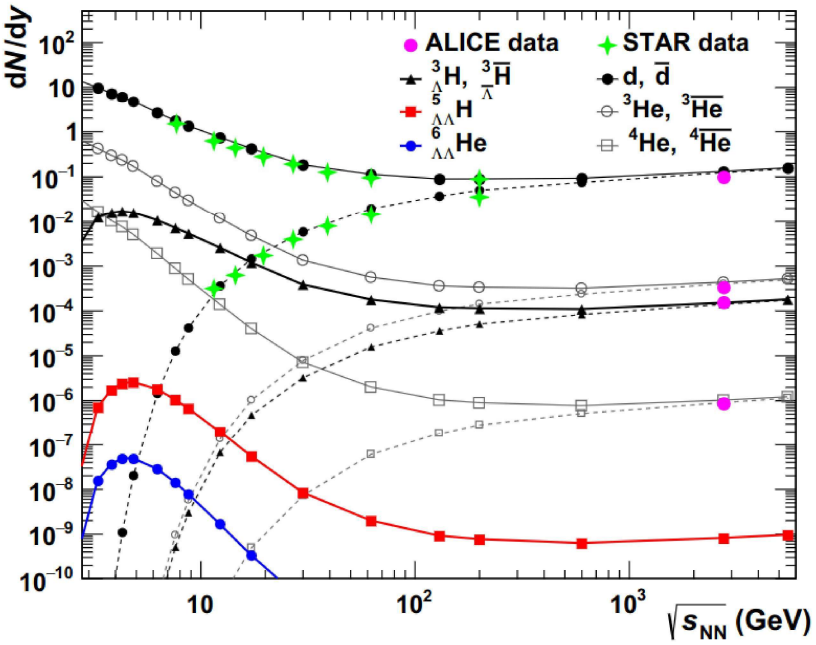

Figure 5.2 The comparison between thermal predictions and the measured (anti)nuclei production on the energy spectrum. The figure is adopted from Ref. (Dönigus, 2020)

Despite its simplicity and successful predictions of cluster yields, the thermal prescription ultimately assumes the formation of nuclei directly from the chemical freeze-out stage with $T_{chem} \approx 150$ MeV which is much larger than the binding energies of all (hyper)nuclei, thus raising the questions which mechanisms are realized in nature.

In contrast to the thermal model, the coalescence model assumes that light (anti)nuclei are produced at a later stage, i.e., the kinetic freeze-out (Braun-Munzinger and Dönigus, 2019; Mrówczyński and Słoń, 2020).

5.2.2 Coalescence Model

The coalescence model assumes that light nuclei are formed by the coalescence of nucleons and other light clusters that are sufficiently close in coordinate and momentum space. The coalescence probability depends on the momentum and separation of the nucleons or clusters.

The model describes the formation of composited particles in the late stage of the collision - first, all resonances decay into nucleons, then nucleons coalesce into nuclei at the freeze-out stage. There are many types of coalescence models (Hagedorn, 1960; Butler and Pearson, 1963; Bond et al., 1977; Csernai and Kapusta, 1986; Sato and

Yazaki, 1981; Hillery et al., 1984; Danielewicz and Schuck, 1992; Mrowczynski, 1992; Kittiratpattana et al., 2020). The model states that a pair of final-state (anti)nucleons that are carrying similar momenta can coalesce to form a deuteron or an anti-deuteron with total momentum **P** as shown in figure 5.3. The nucleus-nucleus collision creates a fireball which emits protons, neutrons, and many other particles out. In the case where an emitted proton and neutron have similar momenta, they will be localized and formed into a deuteron. Different formulations for the coalescence rate are possible. In this section, we will discuss the problems with the simple coalescence model and present the more considerate treatment for the model.

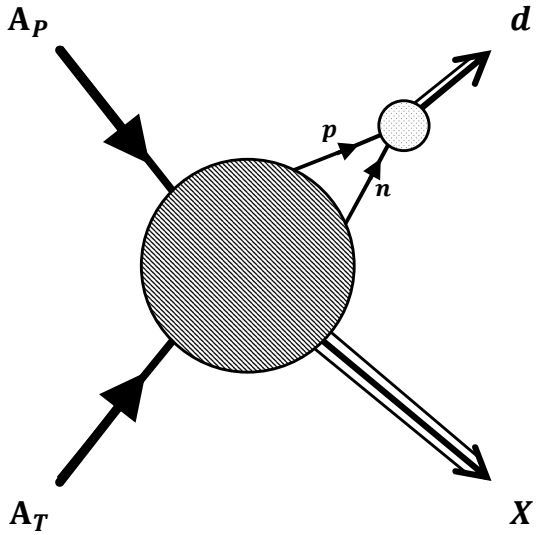

Figure 5.3 The schematic for a particle production and cluster formation from a colliding projectile nucleus A_P and a target nucleus A_T. In the coalescence model, the free streaming neighbor of p and n pair after flying a certain distance will coalesce and form a deuteron outside of the fireball. The rest of the momentum is represented by X. This coalescence process happens at kinetic freeze-out. The figure is adopted from Ref. (Kapusta, 1980)

Simple Momentum Coalescence

The coalescence model for relativistic nuclear collisions was developed from the physical insight provided by proton-nucleus collisions by Butler and Pearson (Butler and Pearson, 1963). Then, Ref. (Schwarzschild and Zupancic, 1963) pointed out that, independent of the detailed production mechanism, the deuteron density $d^3N_d/d\mathbf{P}^3$

should be proportional to the square of the proton density $\left(d^3N_p/d\mathbf{p}^3\right)^2$. The coefficient may be momentum dependent and could be made dependent on the space-time details of the mechanism.

The derivation of the coalescence model for deuterons goes as follows. Let $d^3N_p/d\mathbf{p}^3$ be the invariant momentum space density for nucleons before coalescence into deuterons. We assume that protons and neutrons have equal densities but the formulas can be generalized to include the non-equal cases. The probability of finding one nucleon with momentum p_0 is density times the volume of momentum sphere averaging by the mean of nucleon multiplicity.

$$P = \frac{1}{M}\frac{4\pi}{3}p_0^3\gamma\frac{d^3N_p}{d\mathbf{p}^3} \tag{5.6}$$

where M is the mean nucleon multiplicity. The purely statistical probability for finding two nucleons in the case where $M \ll 1$ and $MP \gg 1$ of this sphere is

$$P_M(2) = \binom{M}{2}P^2(1-P)^{M-2} \tag{5.7}$$

$$\frac{4\pi}{3}p_0^3\gamma\frac{d^3N_d}{d\mathbf{P}^3} = \frac{M^2}{2}\left(\frac{1}{M}\frac{4\pi}{3}p_0^3\gamma\frac{d^3N_p}{d\mathbf{p}^3}\right)^2 \tag{5.8}$$

$$\gamma\frac{d^3N_d}{d\mathbf{P}^3} = \frac{1}{2}\frac{4\pi}{3}p_0^3\left(\gamma\frac{d^3N_p}{d\mathbf{p}^3}\right)^2 \tag{5.9}$$

If we consider the spin (triplets and singlet) and isospin (triplets and singlet) combinations, we obtain,

$$\gamma\frac{d^3N_d}{d\mathbf{P}^3} = 8\frac{3}{4}\frac{4\pi}{3}p_0^3\left(\gamma\frac{d^3N_p}{d\mathbf{p}^3}\right)^2 \tag{5.10}$$

again with deuteron momentum $\mathbf{P} = \mathbf{p}_1 + \mathbf{p}_2$ and assuming that these nucleons approximately carry the same momenta $\mathbf{p}_1 = \mathbf{p}_2 = \mathbf{p}$. From here, one can expresses that whenever two nucleons with correct spin-isospin states are within a momentum sphere with radius p_0 of each other then they will coalesce and form a deuteron. However, it is more common to express the density in the form of the Lorentz invariant.

Thus the coalescence model is usually written as,

$$E\left(\frac{d^3\sigma_d}{dP^3}\right) = B_2\left(\frac{E}{2}\frac{d^3\sigma_p}{dp^3}\right)^2, \tag{5.11}$$

assuming the equality of proton and neutron cross sections. E is the energy of the deuteron where the nucleons are assumed to be E/2. B_2 is a well-known coalescence parameter which is used and measured by most experiments related to the coalescence model. Still, B_2 also contains the proportionality to the unknown p_0. However, the physical interpretation of radius p_0 is still questionable (Butler and Pearson, 1963; Schwarzschild and Zupancic, 1963; Gutbrod et al., 1976; Bond et al., 1977; Sato and Yazaki, 1981; Gyulassy et al., 1983; Csernai and Kapusta, 1986; Mrowczynski, 1990). Because this parameter could not be expressed with any dependencies on the collision initial conditions, e.g., the target/projectile size, beam energy, impact parameter etc. However, based on this proportionality, a similar relation between p_0 and the volume V from the thermal model can be drawn,

$$\frac{d^3N_d}{dP^3} = \frac{3}{4}\frac{(2\pi)^3}{V}\frac{d^3N_p}{dp_1^3}\frac{d^3N_n}{dp_2^3}. \tag{5.12}$$

The weighting factor of 3/4 averages the spin multiplicity per nucleon-nucleon bound state. In Lorentz invariant density form, this is:

$$\left(\gamma\frac{d^3N_d}{dp^3}\right) = 8\frac{3}{4}\frac{(2\pi)^3}{V}\frac{1}{\gamma}\left(\gamma\frac{d^3N_p}{dp^3}\right)^2. \tag{5.13}$$

Comparing this the Eq. (5.10) with the thermal model Eq. (5.13), we get the relation with p_0,

$$\frac{4}{3}\pi p_0^3 = \frac{1}{\gamma}\frac{(2\pi)^3}{V} \tag{5.14}$$

According to this naive relation, p_0 seems to be inversely proportional to the thermal volume V and the Lorentz factor γ. One can see that p_0 can now be understood as the coalescence parameter B_A which is expected to have a direct connection with the volume as $B_A \propto \left(\frac{1}{V}\right)^{A-1}$. However, the interpretations of the volume from the thermal model and the coalescence model are not the same. The latter one refers to the volume of homogeneity of the emission source which is in line with the volume from

HBT interferometry (Kapusta, 1980; Ackermann et al., 2003; Csorgo et al., 2006).

Because of its simplicity, this model fails to describe the antideuteron invariant yield at Si+Au in the AGS experiment E802 (Aoki et al., 1992). Figure 5.4 shows the invariant cross section of the negative charged particles, i.e., π^-, K^-, $\bar{p}$, and antideuterons $\bar{d}$. The anticipated cross section ratio of antideuteron to antiproton squared according to the coalescence model is actually 5 — 10 times smaller than the ratio obtained from normal deuteron.

The coalescence model can be upgraded with more explicit descriptions of the phase-space correlation which can incorporate quantum mechanical considerations. An approach for a better description of the antinuclei yields has been suggested by (Mrowczynski, 1993) which we have adopted in this studies the in previous chapter Ch. IV.

Analytic Coalescence Models

The simple coalescence model does not provide any insights into the dynamics of nucleon clustering. It does not predict a numerical value for the coalescence parameter p_0 in Eq. (5.10) or how coalescence parameters depend on system size, centrality or beam energy. Moreover, it does not allow one to extract useful information of nuclear matter properties. Therefore, there was a clear need for a dynamical basis for the coalescence model.

These models generally are based on based on the density matrix of the source (Feynman, 2018; Shuryak and Torres-Rincon, 2020) or the equivalent Wigner function formalism (Hillery et al., 1984), where the quantum effects are incorporated inside the wavefunction calculated with and without potential. In this approach, the coalescence yield is governed by the wavefunction of the state formed by coalescence, typically approximated by a Gaussian function or Hulthén wavefunction (with Yukawa potential) (Zhaba, 2017).

This approach allows us to study the coalescence parameter and cluster yields and to estimate their structure and their underlying interaction (for example ΛN in hypertriton) from different factors (Nagels et al., 1977; Nagels et al., 1979; Shinmura et al., 1984; Fujiwara et al., 1996a; Fujiwara et al., 1996b; Nemura et al., 2000).

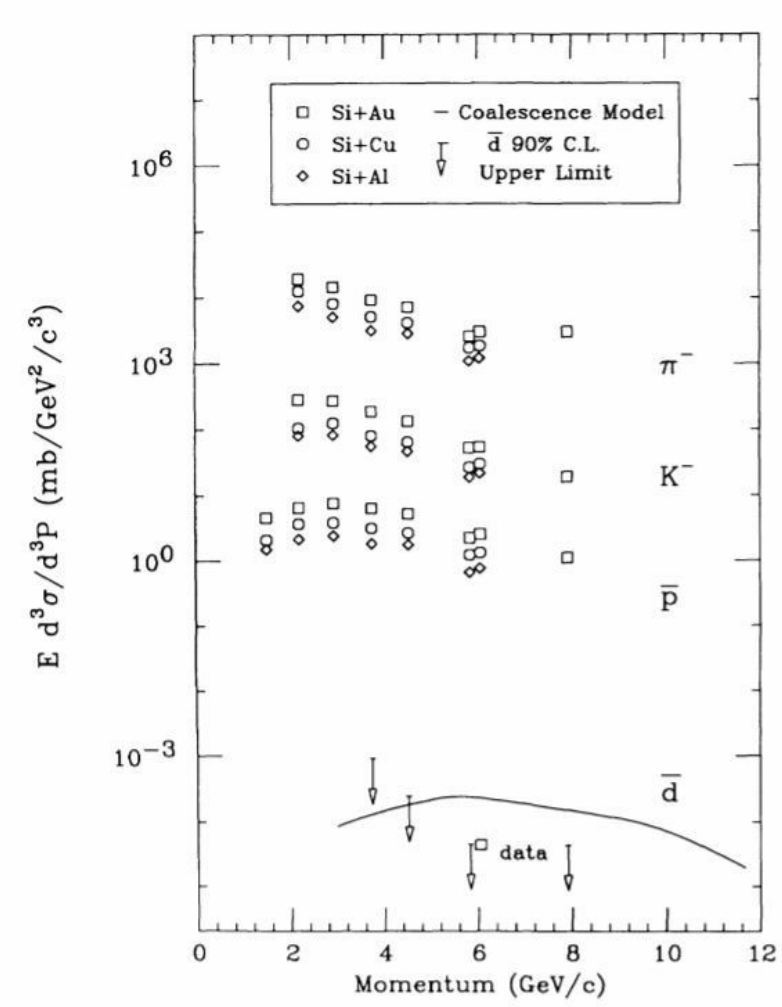

Figure 5.4 The invariant cross section of π^-, K^-, $\bar{p}$ and $\bar{d}$ from Si+Al, Si+Cu, and Si+Au collisions. The solid-line represents the $\bar{d}$'s predicted by coalescence model. The measured $\bar{d}$ and the instrumental upper limit are represented by the square open symbol at 6.1 GeV and down arrow symbols (Aoki et al., 1992).

Wigner's Function

According to the rules of statistical quantum mechanics, the number of created deuterons with momentum $\vec{P}_d$ is given by projecting the deuteron density matrix onto the two-nucleon density matrix ρ_d in the fireball at freeze-out:

$$\frac{d^3N_d}{d\vec{P}_d} \propto \int d^3\vec{x}_1 d^3\vec{x}_2 d^3\vec{x'}_1 d^3\vec{x'}_2 \rho_d\left(\vec{x}_1, \vec{x}_2; \vec{x'}_1, \vec{x'}_2\right) \times \rho_{pn}\left(\vec{x}_1, \vec{x}_2; \vec{x'}_1, \vec{x'}_2\right) \tag{5.15}$$

The two-nucleon spatial density matrix ρ_{pn} in the fireball is not known and has to be approximated. We assume that at freeze-out the nucleons are uncorrelated, i.e., $\rho_{pn}\left(\vec{x}_1, \vec{x}_2; \vec{x'}_1, \vec{x'}_2\right) \approx \rho_p\left(\vec{x}_1, \vec{x'}_1\right)\rho_n\left(\vec{x}_2, \vec{x'}_2\right)$. In order to translate a single particle density matrix into phase-space density representation, the Wigner transformation is needed with new relative coordinates $\vec{r} \equiv \left(\vec{x}_i + \vec{x'}_i\right)/2$ and $\vec{R} = \vec{x}_i - \vec{x'}_i$,

$$f_i\left(\vec{r}_i, \vec{p}_i\right) = \int d^3\vec{R}_i \exp\left(i\vec{p}_i \cdot \vec{R}_i\right) \rho_i\left(\vec{r}_i + \vec{R}_i/2, \vec{r}_i - \vec{R}_i/2\right), \tag{5.16}$$

where $f_i\left(\vec{r}_i, \vec{p}_i\right)$ is the single-particle Wigner function. This is also applicable to the density matrix of the deuteron. The Wigner transformation of clusters are usually expressed within the wavefunction form since we can calculate and impose physical structure on the wavefunction. We have,

$$\mathcal{W}_d = \int d^3\vec{R} \Psi_d\left(\vec{r} + \frac{\vec{R}}{2}\right) \Psi_d^*\left(\vec{r} - \frac{\vec{R}}{2}\right) \exp\left(-i\vec{p} \cdot \vec{R}\right), \tag{5.17}$$

where $\Psi\left(\vec{r}\right)$ is the cluster wavefunction, i.e., deuteron wavefunction or a relative wavefunction of the constituents.

With all of these ingredients, we now can formulate the cluster yields of mass A in the expression of the overlapping nucleons phase-space functions $f_i\left(\vec{r}_i, \vec{p}_i\right)$ with the probability of the reaction determined by Wigner transformation of the cluster matrix:

$$N_A = g_A \int \left[\prod_i^A d^3\vec{r}_i d^3\vec{p}_i f_i\left(\vec{r}_i, \vec{p}_i\right)\right] \mathcal{W}_A\left(\vec{r}, \vec{p}\right), \tag{5.18}$$

where $\mathcal{W}_A(\vec{r}, \vec{p})$ is the so-called Wigner transformation function and g_A is the spin-isospin degeneracy. Typically the relative wavefunction or cluster wavefunction $\Psi(\vec{r})_A$ is usually assumed to be the spherical harmonic-oscillator wavefunction which leads to the expression of:

$$\mathcal{W}_A(\vec{r}, \vec{q}) = 8^{A-1} \exp\left[-\sum_{i=1}^{A}\left(\frac{\vec{R}_i^2}{\sigma_i^2} + \sigma_i^2 \vec{q}_i^2\right)\right], \tag{5.19}$$

The parameter σ_i is associated with the root-mean-square (rms) radius of coalesced nuclei.

Besides this simple Wigner's transformation, one can also apply the same idea, adopted from density matrix considerations, with different assumptions as, e.g., suggested by S. Mrówczyński which not only assumes a simple Gaussian model but also uses the more realistic Hulthén wavefunction (well described at low energies, but does not impact on the final results much). We will discuss this model in more detail in Ch.IV.

5.2.3 Dynamical Model

To consider dynamical effects for cluster productions, we generally integrate cluster formation into the event generators, mostly the transport models and/or hydrodynamical models.

UrQMD + Box Coalescence

The coalescence model is integrated into UrQMD with the concept of box coalescence, i.e., the phase-space coordinates (positions and momenta) of all nucleons are extracted at kinetic freeze-out, a criterion is then established to determine if nucleons are close enough in phase space to form a nucleus. This involves both spatial and momentum proximity criteria ΔR and ΔP.

The distance between nucleons is evaluated in the center of mass frame of the nucleons considered for coalescence. This process is repeated iteratively for all nucleons in the system, ensuring that all possible clusters are identified. The final step involves the spin-isospin projection probability to a pair of these proximity nucleons.

In this study, we will use and discuss about this hybrid approach often and in more detailed in the following sections.

PHQMD + MST

In the Quantum Molecular Dynamics (QMD) approach (specifically the PHQMD realization (Aichelin et al., 2020)), nucleons interact through both potentials and collisions. The potential between nucleons is attractive around nuclear ground state densities, and thus, at the end of a heavy-ion reaction, nucleons tend to stay together and form clusters. To identify these clusters, a Minimum Spanning Tree (MST) procedure (Aichelin, 1991) is applied, described as follows:

In the MST algorithm, only coordinate space information is used to identify clusters. A nucleon is considered part of a cluster if its spatial distance to any other nucleon is less than $r_0 = 4$ fm in the local rest frame of the cluster. The distance is calculated by a Lorentz transformation from the computational frame to the local rest frame, and the cut-off distance is chosen according to the range of the potential in PHQMD. Nucleons more distant than the cut-off distance are assumed not to be bound by the attractive nuclear interaction of that specific cluster.

The main advantage of the MST method is that it allows the identification of clusters at any time during the system's evolution. While the coalescence mechanism combines nucleons into deuterons at the kinetic freeze-out hypersurface, the MST method identifies clusters dynamically as the clusters are created by potential interactions at different stages of the evolution.

SMASH + Nucleon/Pion Catalyses

While coalescence and thermal models offer valuable frameworks for understanding cluster formation, recent developments suggest a more nuanced picture. Here, we discuss the SMASH (Simulating Many Accelerated Strongly-interacting Hadrons) transport model and its potential to capture the complexity of deuteron production.

Similar to the URQMD model, SMASH (Weil et al., 2016) simulates heavy-ion collisions by accounting for various interaction types based on the mean-field BUU numerical code. However, SMASH also includes multiple reactions like three-body collisions (Staudenmaier et al., 2021). It also directly calculates or fits inelastic cross sections, incorporating the detailed balance relationship between deuteron creation and destruction reactions. Recent advancements in SMASH include a stochastic collision implementation coupled with a hydrodynamic afterburner, allowing for the calculation of these multiple reactions.

As highlighted in Ref. (Oliinychenko, 2021; Liu et al., 2020), observed deuteron

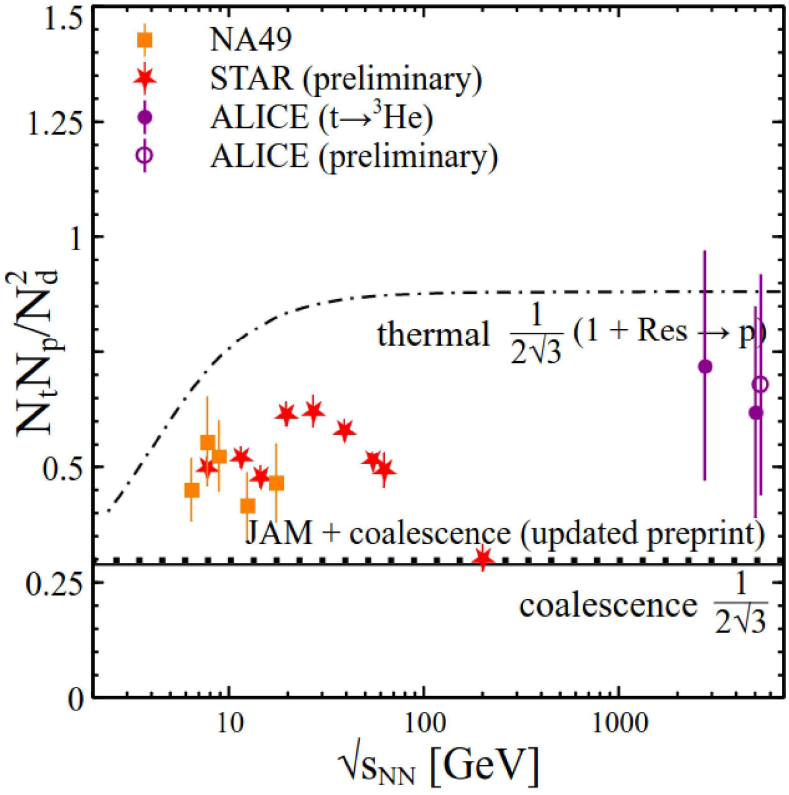

Figure 5.5 The Comparison of the tp/d^2 ratio from two cluster formation mechanisms of thermal (dashed line) and simple coalescence model (solid line) with experimental data (symbols).

production might not be solely explained by either coalescence or thermal models. The thermal model suggests cluster formation directly at the chemical freeze-out stage, alongside resonances and decays. In contrast, the coalescence model proposes cluster formation at the later kinetic freeze-out, with constituent nucleons influenced by resonances and decays only at final state.

Figure 5.5 illustrates how experimental data for the tp/d^2 ratio falls somewhere between the predictions of these two models. This suggests that cluster formation likely involves a combination of mechanisms working together.

The formation and disintegration of deuterons is catalyzed by reactions involving pions or nucleons, such as:

$$\pi d \leftrightarrow \pi np,$$
$$Nd \leftrightarrow Nnp,$$
$$\overline{N}d \leftrightarrow \overline{N}np,$$
$$\pi d \leftrightarrow NN\ .$$

Additionally, rate reactions for these particle-deuteron interactions are included in the model. Studies suggest that $Nd \leftrightarrow Npn$ dominates at lower beam energies (4 — 5 GeV), while $\pi d \leftrightarrow \pi pn$ becomes more significant at higher energies (7.7 GeV).

SMASH's nucleon/pion catalysis model suggests that deuterons, often described as "snowballs in hell" within the thermal model analogy, do not simply survive from the chemical freeze-out ($T_{chem} \approx 150$ MeV) to the kinetic freeze-out. Instead, they are likely continuously disintegrated and re-created at similar rates, maintaining a state of relative equilibrium with the surrounding nucleons (Oliinychenko et al., 2021).

5.2.4 Multifragmentation

The multifragmentation model (Bondorf et al., 1995) describes the breakup of a highly excited nucleus into smaller fragments, i.e., (light)(hyper)nuclei, based on their mass A and charge Z. It can be viewed as a liquid-gas phase transition analogy applied to excited nuclear matter (Barz et al., 1986).

The excitation energy involved in the heavy-ion collisions is typically ranging between $\epsilon^* \simeq 1$ — 10 MeV/nucleon. At low excitation energies $\epsilon^* \approx 1$ MeV/nucleon, the nuclear system can be fully described with the liquid-drop model as the baryon density is then close to the saturation density $\rho_0 \approx 0.15$ fm^3. When the system

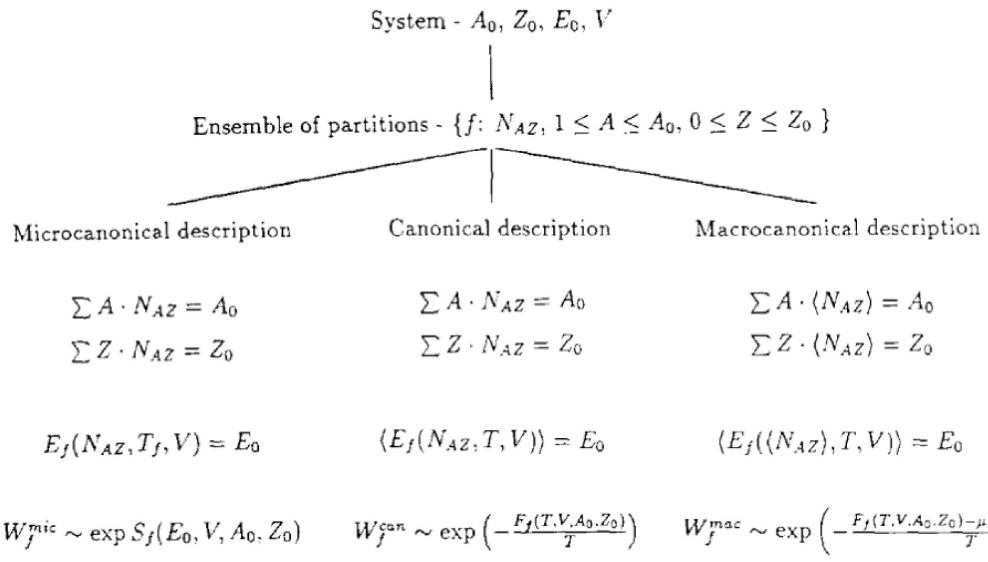

Figure 5.6 Different statistical ensembles used for describing the breakup of a nuclear system with partition f (Bondorf et al., 1995; Fai and Randrup, 1983; Gross, 1984).

reaches higher excitation energies, the baryon density becomes smaller $\rho < \rho_0$, the nuclear system can be excited and realized as a droplet as described by the liquid-drop model (if $\rho \lesssim \rho_0/2$). At this stage, attractive nuclear force dominates and favoring clusterization, leading to so-called pre-fragments. Finally, when the excitation energy is high enough $\epsilon^* \simeq 5$ — 8 MeV/nucleon, i.e., higher than most total binding energies of (light) nuclei, the compound (excited) nuclei begin to loosen as long-range Coulomb repulsion becomes important. In the excited nuclear system, the primary fragments cannot hold together anymore and evaporation-like decay mechanisms occur, resulting in the explosive break-up, This process could occur multiple times reducing the excitation energies of the fragments and emitting multiple fragments, a process known as multifragmentation.

Considering a large ensemble of final fragments and assuming local equilibrium with constraints from nuclear configurations and Coulomb energies, we can describe multifragmentation statistically. Figure 5.6 illustrates different statistical ensembles used for describing the breakup of the nuclear system, all conserving total mass (A_0), charge (Z_0), and energy (E_0).

The total energy of a fragment partition (f) can be expressed as:

$$E_f(T, V) = E_f^{tr}(T, V) + \sum_{(A,Z)} E_{(A,Z)}(T, V) + E_0^C(V) \tag{5.20}$$

The first term (E_f^{tr}) describes the translational and rotational motion of fragments. The second term accounts for the internal excitation energy and clusterization energy of individual fragments (A, Z). The third term (E_0^C) represents the total Coulomb energy.

The final fragment multiplicities can be determined by considering the system at thermal equilibrium, where the number of microscopic states leading to a specific partition is governed by its entropy (S_f).

The multifragmentation process can be visualized in three stages: (I) The initial non-equilibrium stage, this stage leads to the production of an intermediate highly-excited nuclear system. It is important to note that there is no clear or unified model to describe the initial non-equilibrium stage. Additionally, the final multiplicity of the fragment nuclei is highly sensitive to the initial conditions. (II) Fragment formation and breakup: Breakup of the system into separate fragments through a complex interplay of nuclear and Coulomb forces. (III) Coulomb Propagation and de-excitation: Hot fragments interact via Coulomb repulsion and undergo de-excitation through various mechanisms.

Since the initial non-equilibrium stage lacks a complete theoretical description, a hybrid modeling approach is often employed. This combines dynamical models (e.g., transport models like UrQMD) to describe the initial stages (system size, participants, energy density) with statistical multifragmentation models to describe fragment formation at later stages when the system approaches equilibrium. The implementation of such hybrid models will be discussed in Chapter VIII.